



RESEARCH ARTICLE

10.1029/2019EA000582

## A 3-Year Sample of Almost 1,600 Elves Recorded Above South America by the Pierre Auger Cosmic-Ray Observatory

**Key Points:**

- Elves are observed in Argentina, which is known for severe convective thunderstorms
- A UV fluorescence detector, continuing operations through 2025, has a viewing footprint of 3 million km<sup>2</sup>
- Cameras with 10 MHz frame rate reveal the internal EMP structure generated by lightning strokes

**Supporting Information:**

- Data Set S1

**Correspondence to:**

R. Engel,  
auger\_spokespersons@fnal.gov

**Citation:**

Aab, A., Abreu, P., Aglietta, M., Albuquerque, I. F. M., Albury, J. M., Allekotte, I., et al. (2020). A 3-year sample of almost 1,600 elves recorded above South America by the Pierre Auger Cosmic-Ray Observatory. *Earth and Space Science*, 7, e2019EA000582. <https://doi.org/10.1029/2019EA000582>

Received 30 JAN 2019








Accepted 22 JAN 2020

Accepted article online 21 FEB 2020

A. Aab<sup>1</sup>, P. Abreu<sup>2</sup>, M. Aglietta<sup>3,4</sup>, I. F. M. Albuquerque<sup>5</sup>, J. M. Albury<sup>6</sup>, I. Allekotte<sup>7</sup>, A. Almela<sup>8,9</sup>, J. Alvarez Castillo<sup>10</sup>, J. Alvarez-Muñiz<sup>11</sup>, G. A. Anastasi<sup>12,13</sup>, L. Anchordoqui<sup>14</sup>, B. Andrada<sup>8</sup>, S. Andringa<sup>2</sup>, C. Aramo<sup>15</sup>, H. Asorey<sup>7,16</sup> , P. Assis<sup>2</sup> , G. Avila<sup>17,18</sup>, A. M. Badescu<sup>19</sup>, A. Bakalova<sup>20</sup>, A. Balaceanu<sup>21</sup>, F. Barbato<sup>15,22</sup>, R. J. Barreira Luz<sup>2</sup>, S. Baur<sup>23</sup>, K. H. Becker<sup>24</sup>, J.A. Bellido<sup>6</sup>, C. Berat<sup>25</sup>, M. E. Bertaina<sup>4,26</sup> , X. Bertou<sup>7</sup>, P. L. Biermann<sup>27</sup>, J. Biteau<sup>28</sup>, S. G. Blaess<sup>6</sup>, A. Blanco<sup>2</sup>, J. Blazek<sup>20</sup>, C. Bleve<sup>29,30</sup>, M. Boháčová<sup>20</sup>, D. Boncioli<sup>12,13</sup>, C. Bonifazi<sup>31</sup>, N. Borodai<sup>32</sup>, A. M. Botti<sup>8</sup>, J. Brack<sup>33</sup>, T. Bretz<sup>34</sup>, A. Bridgeman<sup>35</sup>, F. L. Brichele<sup>34</sup>, P. Buchholz<sup>36</sup>, A. Bueno<sup>37</sup>, S. Buitink<sup>38</sup>, M. Buscemi<sup>39,40</sup>, K. S. Caballero-Mora<sup>41</sup>, L. Caccianiga<sup>42</sup>, L. Calcagni<sup>43</sup>, A. Cancio<sup>8,9</sup>, F. Canfora<sup>1,44</sup>, J. M. Carceller<sup>37</sup>, R. Caruso<sup>39,40</sup>, A. Castellina<sup>3,4</sup>, F. Catalani<sup>45</sup>, G. Cataldi<sup>30</sup>, L. Cazon<sup>2</sup>, M. Cerda<sup>17</sup>, J. A. Chinellato<sup>46</sup>, J. Chudoba<sup>20</sup>, L. Chytka<sup>47</sup>, R.W. Clay<sup>6</sup>, A. C. Cobos Cerutti<sup>48</sup>, R. Colalillo<sup>15,22</sup>, A. Coleman<sup>49</sup>, M. R. Coluccia<sup>29,30</sup>, R. Conceição<sup>2</sup>, A. Condorelli<sup>12,13</sup>, G. Consolati<sup>50,51</sup>, F. Contreras<sup>17,18</sup>, M. J. Cooper<sup>6</sup>, S. Coutu<sup>49</sup>, C. E. Covault<sup>52</sup>, B. Daniel<sup>46</sup>, S. Dasso<sup>53,54</sup> , K. Daumiller<sup>23</sup>, B. R. Dawson<sup>6</sup>, J. A. Day<sup>6</sup>, R. M. de Almeida<sup>55</sup>, S. J. de Jong<sup>1,44</sup>, G. Mauro<sup>1,44</sup>, J. R. T. de Mello Neto<sup>31,56</sup>, I. Mitri<sup>12,13</sup>, J. de Oliveira<sup>55</sup>, F. O. de Oliveira Salles<sup>57</sup>, V. de Souza<sup>58</sup>, J. Debatin<sup>35</sup>, M. del Río<sup>18</sup>, O. Deligny<sup>28</sup>, N. Dhital<sup>32</sup>, M. L. Díaz Castro<sup>46</sup>, F. Diogo<sup>2</sup>, C. Dobrigkeit<sup>46</sup>, J. C. D'Oliveiro<sup>10</sup>, Q. Dorosti<sup>36</sup>, R. C. dos Anjos<sup>59</sup>, M. T. Dova<sup>43</sup>, A. Dundovic<sup>60</sup>, J. Ebr<sup>20</sup>, R. Engel<sup>35</sup>, M. Erdmann<sup>34</sup>, C. O. Escobar<sup>61</sup>, A. Etchegoyen<sup>8,9</sup>, H. Falcke<sup>1,44,62</sup>, J. Farmer<sup>63</sup>, G. Farrar<sup>64</sup>, A. C. Fauth<sup>46</sup>, N. Fazzini<sup>61</sup>, F. Feldbusch<sup>65</sup>, F. Fenu<sup>4,26</sup>, L. P. Ferreyro<sup>8</sup>, J. M. Figueira<sup>8</sup>, A. Filipčić<sup>66,67</sup>, M. M. Freire<sup>68</sup>, T. Fujii<sup>63,69</sup>, A. Fuster<sup>8,9</sup>, B. García<sup>48</sup> , H. Gemmeke<sup>65</sup>, A. Gherghel-Lascu<sup>21</sup>, P. L. Ghia<sup>28</sup>, U. Giaccari<sup>57</sup>, M. Giammarchi<sup>50</sup>, M. Giller<sup>70</sup>, D. Glas<sup>71</sup>, J. Glombitza<sup>34</sup>, F. Gobbi<sup>17</sup>, G. Golup<sup>7</sup>, M. Gómez Berisso<sup>7</sup>, P. F. Gómez Vitale<sup>17,18</sup>, J. P. Gongora<sup>17</sup>, N. González<sup>8</sup>, I. Goos<sup>7,23</sup>, D. Góra<sup>32</sup>, A. Gorgi<sup>3,4</sup>, M. Gottowik<sup>24</sup>, T. D. Grubb<sup>6</sup>, F. Guarino<sup>15,22</sup>, G. P. Guedes<sup>72</sup>, E. Guido<sup>4,26</sup>, R. Halliday<sup>52</sup>, M. R. Hampel<sup>8</sup>, P. Hansen<sup>43</sup>, D. Harari<sup>7</sup>, T. A. Harrison<sup>6</sup>, V. M. Harvey<sup>6</sup>, A. Haungs<sup>23</sup>, T. Hebbeker<sup>34</sup>, D. Heck<sup>23</sup>, P. Heimann<sup>36</sup>, G. C. Hill<sup>6</sup>, C. Hojvat<sup>61</sup>, E. M. Holt<sup>35</sup>, P. Homola<sup>32</sup>, J. R. Hörandel<sup>1,44</sup>, P. Horvath<sup>47</sup>, M. Hrabovský<sup>47</sup>, T. Huege<sup>23,38</sup>, J. Hulsman<sup>8,23</sup>, A. Insolia<sup>39,40</sup>, P. G. Isar<sup>73</sup>, I. Jandt<sup>24</sup>, J. A. Johnsen<sup>74</sup>, M. Josebachuili<sup>8</sup>, J. Jurysek<sup>20</sup>, A. Kääpä<sup>24</sup>, K. H. Kampert<sup>24</sup> , B. Keilhauer<sup>23</sup>, N. Kemmerich<sup>5</sup>, J. Kemp<sup>34</sup>, H. O. Klages<sup>23</sup>, M. Kleifges<sup>65</sup> , J. Kleinfeller<sup>17</sup>, R. Krause<sup>34</sup>, D. Kuempel<sup>24</sup>, G. Kukec Mezek<sup>67</sup>, A. Kuotb Awad<sup>35</sup>, B. L. Lago<sup>75</sup>, D. LaHurd<sup>52</sup>, R. G. Lang<sup>58</sup>, R. Legumina<sup>70</sup>, M. A. Leigui de Oliveira<sup>76</sup>, V. Lenok<sup>23</sup>, A. Letessier-Selvon<sup>77</sup>, I. Lhenry-Yvon<sup>28</sup>, O. C. Lippmann<sup>57</sup>, D. Lo Presti<sup>39,40</sup> , L. Lopes<sup>2</sup>, R. López<sup>78</sup>, A. López Casado<sup>11</sup>, R. Lorek<sup>52</sup>, Q. Luce<sup>28</sup>, A. Lucero<sup>8</sup>, M. Malacari<sup>63</sup>, G. Mancarella<sup>29,30</sup>, D. Mandat<sup>20</sup>, B. C. Manning<sup>6</sup>, P. Mantsch<sup>61</sup>, A. G. Mariazzi<sup>43</sup>, I. C. Mariş<sup>79</sup>, G. Marsella<sup>29,30</sup>, D. Martello<sup>29,30</sup>, H. Martinez<sup>80</sup>, O. Martínez Bravo<sup>78</sup>, M. Mastrodicasa<sup>13,81</sup>, H. J. Mathes<sup>23</sup>, S. Mathys<sup>24</sup>, J. Matthews<sup>82</sup>, G. Matthiae<sup>83,84</sup>, E. Mayotte<sup>24</sup>, P. O. Mazur<sup>61</sup>, G. Medina-Tanco<sup>10</sup>, D. Melo<sup>8</sup>, A. Menshikov<sup>65</sup>, K.-D. Merenda<sup>74</sup> , S. Michal<sup>47</sup>, M. I. Micheletti<sup>68</sup>, L. Middendorf<sup>34</sup>, L. Miramonti<sup>42,50</sup>, B. Mitrica<sup>21</sup>, D. Mockler<sup>35</sup>, S. Mollerach<sup>7</sup>, F. Montanet<sup>25</sup>, C. Morello<sup>3,4</sup>, G. Morlino<sup>12,13</sup>, M. Mostafá<sup>49</sup>, A. L. Müller<sup>8,23</sup>, M. A. Muller<sup>46,85</sup>, S. Müller<sup>35</sup>, R. Mussa<sup>4</sup>, L. Nellen<sup>10</sup> , P. H. Nguyen<sup>6</sup>, M. Niculescu-Oglinza<sup>21</sup>, M. Niechciol<sup>36</sup>, D. Nitz<sup>86,87</sup>, D. Nosek<sup>88</sup>, V. Novotny<sup>88</sup>, L. Noža<sup>47</sup>, A. Nucita<sup>29,30</sup>, L.A. Núñez<sup>16</sup> , A. Olinto<sup>63</sup>, M. Palatka<sup>20</sup>, J. Pallotta<sup>89</sup>, M. P. Panetta<sup>29,30</sup>, P. Papenbreer<sup>24</sup>, G. Parente<sup>11</sup>, A. Parra<sup>78</sup>, M. Pech<sup>20</sup>, F. Pedreira<sup>11</sup>, J. Pękala<sup>32</sup>, R. Pelayo<sup>90</sup>, J. Peña-Rodríguez<sup>16</sup>, L. A. S. Pereira<sup>46</sup>, M. Perlin<sup>8</sup>, L. Perrone<sup>29,30</sup>, C. Peters<sup>34</sup>, S. Petrerá<sup>12,13</sup>, J. Phuntsok<sup>49</sup>, T. Pierog<sup>23</sup>, M. Pimenta<sup>2</sup>, V. Pirronello<sup>39,40</sup>, M. Platino<sup>8</sup>, J. Poh<sup>63</sup>, B. Pont<sup>1</sup>, C. Porowski<sup>32</sup>, R. R. Prado<sup>58</sup>, P. Privitera<sup>63</sup>, M. Prouza<sup>20</sup>, A. Puyleart<sup>86</sup>, S. Querchfeld<sup>24</sup>, S. Quinn<sup>52</sup> , R. Ramos-Pollán<sup>16</sup>, J. Rautenberg<sup>24</sup>, D. Ravignani<sup>8</sup>, M. Reininghaus<sup>23</sup>, J. Ridky<sup>20</sup>, F. Riehn<sup>2</sup>, M. Risse<sup>36</sup>, P. Ristori<sup>89</sup>, V. Rizi<sup>13,81</sup>, W. Rodrigues de Carvalho<sup>5</sup>, J. Rodriguez Rojo<sup>17</sup>, M. J. Roncoroni<sup>8</sup>, M. Roth<sup>23</sup>, E. Roulet<sup>7</sup>, A. C. Rovero<sup>53</sup>, P. Ruehl<sup>36</sup>, S. J. Saffi<sup>6</sup>, A. Saftoiu<sup>21</sup>, F. Salamida<sup>13,81</sup>, H. Salazar<sup>78</sup>, G. Salina<sup>84</sup>

©2020. The Authors.

This is an open access article under the terms of the Creative Commons Attribution License, which permits use, distribution and reproduction in any medium, provided the original work is properly cited.

J. D. Sanabria Gomez<sup>16</sup>, F. Sánchez<sup>8</sup>, E. M. Santos<sup>5</sup>, E. Santos<sup>20</sup>, F. Sarazin<sup>74</sup>, R. Sarmento<sup>2</sup>, C. Sarmiento-Cano<sup>8</sup>, R. Sato<sup>17</sup>, P. Savina<sup>29,30</sup>, M. Schauer<sup>24</sup>, V. Scherini<sup>30</sup>, H. Schieler<sup>23</sup>, M. Schimassek<sup>35</sup>, M. Schimp<sup>24</sup>, F. Schlüter<sup>23</sup>, D. Schmidt<sup>35</sup>, O. Scholten<sup>38,91</sup> , P. Schovánek<sup>20</sup>, F. G. Schröder<sup>23,92</sup>, S. Schröder<sup>24</sup>, J. Schumacher<sup>34</sup>, S. J. Sciutto<sup>43</sup>, M. Scornavacche<sup>8</sup>, R. C. Shellard<sup>57</sup>, G. Sigl<sup>60</sup>, G. Silli<sup>8,23</sup>, O. Sima<sup>21,93</sup>, R. Šmída<sup>63</sup>, G.R. Snow<sup>94</sup>, P. Sommers<sup>49</sup>, J. F. Soriano<sup>14</sup>, J. Souchard<sup>25</sup>, R. Squartini<sup>17</sup>, D. Stanca<sup>21</sup>, S. Stanić<sup>67</sup> , J. Stasielak<sup>32</sup>, P. Stassi<sup>25</sup>, M. Stolpovskiy<sup>25</sup>, A. Streich<sup>35</sup>, F. Suarez<sup>8,9</sup>, M. Suárez-Durán<sup>16</sup> , T. Sudholz<sup>6</sup>, T. Suomijärvi<sup>28</sup>, A.D. Supanitsky<sup>8</sup>, J. Šupík<sup>47</sup>, Z. Szadkowski<sup>71</sup>, A. Taboada<sup>23</sup>, O. A. Taborda<sup>7</sup>, A. Tapia<sup>95</sup>, C. Timmermans<sup>1,44</sup>, C. J. Todero Peixoto<sup>45</sup>, B. Tomé<sup>2</sup>, G. Torralba Elipse<sup>11</sup>, A. Travaini<sup>17</sup>, P. Travnicek<sup>20</sup>, M. Trini<sup>67</sup>, M. Tueros<sup>43</sup>, R. Ulrich<sup>23</sup> , M. Unger<sup>23</sup>, M. Urban<sup>34</sup>, J. F. Valdés Galicia<sup>10</sup>, I. Valiño<sup>12,13</sup>, L. Valore<sup>15,22</sup>, P. van Bodegom<sup>6</sup>, A. M. van den Berg<sup>91</sup>, A. van Vliet<sup>1</sup>, E. Varela<sup>78</sup>, B. Vargas Cárdenas<sup>10</sup>, D. Veberič<sup>23</sup> , C. Ventura<sup>56</sup>, I. D. Vergara Quispe<sup>43</sup>, V. Verzi<sup>84</sup>, J. Vicha<sup>20</sup>, L. Villaseñor<sup>78</sup>, J. Vink<sup>96</sup>, S. Vorobiov<sup>67</sup> , H. Wahlberg<sup>43</sup>, A. A. Watson<sup>97</sup>, M. Weber<sup>65</sup>, A. Weindl<sup>23</sup>, M. Wiedeński<sup>71</sup>, L. Wiencke<sup>74</sup> , H. Wilczyński<sup>32</sup>, T. Winchen<sup>38</sup>, M. Wirtz<sup>34</sup>, D. Wittkowski<sup>24</sup>, B. Wundheiler<sup>8</sup>, L. Yang<sup>67</sup>, A. Yushkov<sup>20</sup>, E. Zas<sup>11</sup>, D. Zavrtnik<sup>66,67</sup>, M. Zavrtnik<sup>66,67</sup>, L. Zehrer<sup>67</sup>, A. Zepeda<sup>80</sup>, B. Zimmermann<sup>23</sup>, M. Ziolkowski<sup>36</sup>, Z. Zong<sup>28</sup> and F. Zuccarello<sup>39,40</sup>

<sup>1</sup>IMAPP, Radboud University Nijmegen, Nijmegen, The Netherlands, <sup>2</sup>Laboratório de Instrumentação e Física Experimental de Partículas – LIP and Instituto Superior Técnico – IST, Universidade de Lisboa – UL, Lisboa, Portugal, <sup>3</sup>Osservatorio Astrofisico di Torino (INAF), Torino, Italy, <sup>4</sup>INFN, Sezione di Torino, Torino, Italy, <sup>5</sup>Instituto de Física, Universidade de São Paulo, São Paulo, SP, Brazil, <sup>6</sup>University of Adelaide, Adelaide, South Australia, Australia, <sup>7</sup>Centro Atómico Bariloche and Instituto Balseiro (CNEA-UNCuyo-CONICET), San Carlos de Bariloche, Argentina, <sup>8</sup>Instituto de Tecnologías en Detección y Astropartículas (CNEA, CONICET, UNSAM), Buenos Aires, Argentina, <sup>9</sup>Universidad Tecnológica Nacional – Facultad Regional Buenos Aires, Buenos Aires, Argentina, <sup>10</sup>Universidad Nacional Autónoma de México, México, D.F., México, <sup>11</sup>Instituto Galego de Física de Altas Enerxías (I.G.F.A.E.), Universidad de Santiago de Compostela, Santiago de Compostela, Spain, <sup>12</sup>Gran Sasso Science Institute, L'Aquila, Italy, <sup>13</sup>INFN Laboratori Nazionali del Gran Sasso, Assergi (L'Aquila), Italy, <sup>14</sup>Department of Physics and Astronomy, Lehman College, City University of New York, Bronx, NY, USA, <sup>15</sup>INFN, Sezione di Napoli, Napoli, Italy, <sup>16</sup>Universidad Industrial de Santander, Bucaramanga, Colombia, <sup>17</sup>Observatorio Pierre Auger, Malargüe, Argentina, <sup>18</sup>Observatorio Pierre Auger and Comisión Nacional de Energía Atómica, Malargüe, Argentina, <sup>19</sup>University Politehnica of Bucharest, Bucharest, Romania, <sup>20</sup>Institute of Physics of the Czech Academy of Sciences, Prague, Czech Republic, <sup>21</sup>“Horia Hulubei” National Institute for Physics and Nuclear Engineering, Bucharest-Magurele, Romania, <sup>22</sup>Dipartimento di Fisica “Ettore Pancini”, Università di Napoli “Federico II”, Napoli, Italy, <sup>23</sup>Institut für Kernphysik, Karlsruhe Institute of Technology, Karlsruhe, Germany, <sup>24</sup>Department of Physics, Bergische Universität Wuppertal, Wuppertal, Germany, <sup>25</sup>Université Grenoble Alpes, CNRS, Grenoble Institute of Engineering Université Grenoble Alpes, LPSC-IN2P3, Grenoble, France, <sup>26</sup>Dipartimento di Fisica, Università Torino, Torino, Italy, <sup>27</sup>Max-Planck-Institut für Radioastronomie, Bonn, Germany, <sup>28</sup>Institut de Physique Nucléaire d'Orsay (IPNO), Université Paris-Sud, Université Paris/Saclay, CNRS-IN2P3, Orsay, France, <sup>29</sup>Dipartimento di Matematica e Fisica “E. De Giorgi”, Università del Salento, Lecce, Italy, <sup>30</sup>INFN, Sezione di Lecce, Lecce, Italy, <sup>31</sup>Instituto de Física, Universidade Federal do Rio de Janeiro, Rio de Janeiro, RJ, Brazil, <sup>32</sup>Institute of Nuclear Physics PAN, Krakow, Poland, <sup>33</sup>Colorado State University, Fort Collins, CO, USA, <sup>34</sup>III. Physikalisches Institut A, RWTH Aachen University, Aachen, Germany, <sup>35</sup>Institute for Experimental Particle Physics (ETP), Karlsruhe Institute of Technology, Karlsruhe, Germany, <sup>36</sup>Universität Siegen, Fachbereich 7 Physik – Experimentelle Teilchenphysik, Siegen, Germany, <sup>37</sup>Universidad de Granada and C.A.F.P.E., Granada, Spain, <sup>38</sup>Vrije Universiteit Brussels, Brussels, Belgium, <sup>39</sup>Dipartimento di Fisica e Astronomia, Università di Catania, Catania, Italy, <sup>40</sup>INFN, Sezione di Catania, Catania, Italy, <sup>41</sup>Universidad Autónoma de Chiapas, Tuxtla Gutiérrez, Chiapas, México, <sup>42</sup>Dipartimento di Fisica, Università di Milano, Milano, Italy, <sup>43</sup>IFLP, Universidad Nacional de La Plata and CONICET, La Plata, Argentina, <sup>44</sup>Nationaal Instituut voor Kernfysica in Hoge Energie Fysica (NIKHEF), Science Park, Amsterdam, The Netherlands, <sup>45</sup>Escola de Engenharia de Lorena, Universidade de São Paulo, Lorena, SP, Brazil, <sup>46</sup>IFGW, Universidade Estadual de Campinas, Campinas, SP, Brazil, <sup>47</sup>RCPTM, Palacky University, Olomouc, Czech Republic, <sup>48</sup>Instituto de Tecnologías en Detección y Astropartículas (CNEA, CONICET, UNSAM) and Universidad Tecnológica Nacional – Facultad Regional Mendoza (CONICET/CNEA), Mendoza, Argentina, <sup>49</sup>Pennsylvania State University, University Park, PA, USA, <sup>50</sup>INFN, Sezione di Milano, Milano, Italy, <sup>51</sup>Dipartimento di Scienze e Tecnologie Aerospaziali, Politecnico di Milano, Milano, Italy, <sup>52</sup>Case Western Reserve University, Cleveland, OH, USA, <sup>53</sup>Instituto de Astronomía y Física del Espacio (IAFE, CONICET-UBA), Buenos Aires, Argentina, <sup>54</sup>Departamento de Física and Departamento de Ciencias de la Atmósfera y los Océanos, FCEyN, Universidad de Buenos Aires and CONICET, Buenos Aires, Argentina, <sup>55</sup>EEIMVR, Universidade Federal Fluminense, Volta Redonda, RJ, Brazil, <sup>56</sup>Observatório do Valongo, Universidade Federal do Rio de Janeiro (UFRJ), Rio de Janeiro, RJ, Brazil, <sup>57</sup>Centro Brasileiro de Pesquisas Físicas, Rio de Janeiro, RJ, Brazil, <sup>58</sup>Instituto de

Física de São Carlos, Universidade de São Paulo, São Carlos, SP, Brazil, <sup>59</sup>Universidade Federal do Paraná, Setor Palotina, Palotina, Brazil, <sup>60</sup>II. Institut für Theoretische Physik, Universität Hamburg, Hamburg, Germany, <sup>61</sup>Fermi National Accelerator Laboratory, Batavia, IL, USA, <sup>62</sup>Stichting Astronomisch Onderzoek in Nederland (ASTRON), Dwingeloo, The Netherlands, <sup>63</sup>Enrico Fermi Institute, University of Chicago, Chicago, IL, USA, <sup>64</sup>New York University, New York, NY, USA, <sup>65</sup>Institut für Prozessdatenverarbeitung und Elektronik, Karlsruhe Institute of Technology, Karlsruhe, Germany, <sup>66</sup>Experimental Particle Physics Department, J. Stefan Institute, Ljubljana, Slovenia, <sup>67</sup>Center for Astrophysics and Cosmology (CAC), University of Nova Gorica, Nova Gorica, Slovenia, <sup>68</sup>Instituto de Física de Rosario (IFIR) – CONICET/U.N.R. and Facultad de Ciencias Bioquímicas y Farmacéuticas U.N.R., Rosario, Argentina, <sup>69</sup>Now at the Hakubi Center for Advanced Research and Graduate School of Science, Kyoto University, Kyoto, Japan, <sup>70</sup>Faculty of Astrophysics, University of Łódź, Łódź, Poland, <sup>71</sup>Faculty of High-Energy Astrophysics, University of Łódź, Łódź, Poland, <sup>72</sup>Universidade Estadual de Feira de Santana, Feira de Santana, Brazil, <sup>73</sup>Institute of Space Science, Bucharest-Magurele, Romania, <sup>74</sup>Colorado School of Mines, Golden, CO, USA, <sup>75</sup>Centro Federal de Educação Tecnológica Celso Suckow da Fonseca, Nova Friburgo, Brazil, <sup>76</sup>Universidade Federal do ABC, Santo André, SP, Brazil, <sup>77</sup>Laboratoire de Physique Nucléaire et de Hautes Energies (LPNHE), Universités Paris 6 et Paris 7, CNRS-IN2P3, Paris, France, <sup>78</sup>Benemérita Universidad Autónoma de Puebla, Puebla, México, <sup>79</sup>Université Libre de Bruxelles (ULB), Brussels, Belgium, <sup>80</sup>Centro de Investigación y de Estudios Avanzados del IPN (CINVESTAV), México, D.F., México, <sup>81</sup>Dipartimento di Scienze Fisiche e Chimiche, Università dell'Aquila, L'Aquila, Italy, <sup>82</sup>Louisiana State University, Baton Rouge, LA, USA, <sup>83</sup>Dipartimento di Fisica, Università di Roma "Tor Vergata", Roma, Italy, <sup>84</sup>INFN, Sezione di Roma "Tor Vergata", Roma, Italy, <sup>85</sup>Also at Universidade Federal de Alfenas, Poços de Caldas, Brazil, <sup>86</sup>Michigan Technological University, Houghton, MI, USA, <sup>87</sup>Also at Karlsruhe Institute of Technology, Karlsruhe, Germany, <sup>88</sup>Faculty of Mathematics and Physics, Institute of Particle and Nuclear Physics, Charles University, Prague, Czech Republic, <sup>89</sup>Centro de Investigaciones en Láseres y Aplicaciones, CITEDEF and CONICET, Villa Martelli, Argentina, <sup>90</sup>Unidad Profesional Interdisciplinaria en Ingeniería y Tecnologías Avanzadas del Instituto Politécnico Nacional (UPIITA-IPN), México, D.F., México, <sup>91</sup>KVI – Center for Advanced Radiation Technology, University of Groningen, Groningen, The Netherlands, <sup>92</sup>Bartol Research Institute, Department of Physics and Astronomy, University of Delaware, Newark, DE, USA, <sup>93</sup>Also at Physics Department, University of Bucharest, Bucharest, Romania, <sup>94</sup>University of Nebraska, Lincoln, NE, USA, <sup>95</sup>Universidad de Medellín, Medellín, Colombia, <sup>96</sup>Faculty of Science, Universiteit van Amsterdam, Amsterdam, The Netherlands, <sup>97</sup>School of Physics and Astronomy, University of Leeds, Leeds, UK

**Abstract** Elves are a class of transient luminous events, with a radial extent typically greater than 250 km, that occur in the lower ionosphere above strong electrical storms. We report the observation of 1,598 elves, from 2014 to 2016, recorded with unprecedented time resolution (100 ns) using the fluorescence detector (FD) of the Pierre Auger Cosmic-Ray Observatory. The Auger Observatory is located in the Mendoza province of Argentina with a viewing footprint for elve observations of  $3 \cdot 10^6$  km<sup>2</sup>, reaching areas above the Pacific and Atlantic Oceans, as well as the Córdoba region, which is known for severe convective thunderstorms. Primarily designed for ultrahigh energy cosmic-ray observations, the Auger FD turns out to be very sensitive to the ultraviolet emission in elves. The detector features modified Schmidt optics with large apertures resulting in a field of view that spans the horizon, and year-round operation on dark nights with low moonlight background, when the local weather is favorable. The measured light profiles of 18% of the elve events have more than one peak, compatible with intracloud activity. Within the 3-year sample, 72% of the elves correlate with the far-field radiation measurements of the World Wide Lightning Location Network. The Auger Observatory plans to continue operations until at least 2025, including elve observations and analysis. To the best of our knowledge, this observatory is the only facility on Earth that measures elves with year-round operation and full horizon coverage.

## 1. Introduction

In the 1990s, Inan et al. (1991, 1997) predicted quantitatively that ionospheric heating by electromagnetic pulses (EMPs) originating from lightning strokes would create a transient flash of light expanding radially faster than the speed of light. The first finite-difference time-domain model effectively showed that the energy density of some very low frequency EMPs was sufficient to heat the plasma at the base of the E-layer of the nighttime ionosphere and induce the fluorescence process of molecules (Taranenko et al., 1993). Since, numerous multidimensional simulations have used electromagnetic or “engineering” return stroke models (Baba & Rakov, 2007; Rakov & Uman, 1998) to create the EMP and predict the spatiotemporal structure and brightness of the light emission at the base of the ionosphere (Cho & Rycroft, 2001; Marshall, 2012; Veronis et al., 1999).

The first observation of the “airglow enhancement,” known to be a transient luminous event (TLE), was captured in 1990 using video cameras with a 33-ms time resolution ( $\Delta\tau$ ) aboard the Discovery Space Shuttle (Boeck et al., 1992). Five years later, in 1995, a multichannel photometer ( $\Delta\tau = 15 \mu\text{s}$ ) and two CCDs ( $\Delta\tau = 17 \text{ms}$ ) made the first ground-based observation of Emissions of Light and Very low frequency perturbations due to Electromagnetic pulse Sources, or elve(s) (Fukunishi et al., 1996). The Imager of Sprites and Upper Atmospheric Lightning (ISUAL), launched aboard FORMOSAT-2 in 2004, was the first satellite instrument to make a global survey of elve occurrences (Chern et al., 2003; Mende et al., 2005). Using a CCD imager ( $\Delta\tau = 14 \text{ms}$ ), a spectrophotometer ( $\Delta\tau = 100 \mu\text{s}$ ), and two array photometers ( $\Delta\tau = 5 \mu\text{s}$ ) consisting of one photomultiplier each, ISUAL concluded that the highest density of elves was over the ocean (Chen et al., 2008). In 2008, the Photometric Imager of Precipitated Electron Radiation (PIPER) ( $\Delta\tau = 40 \mu\text{s}$ ) detected elve “doublets,” with two peaks in the photo trace, which were first observed in 1999 by the array of photometers of Fly’s Eye ( $\Delta\tau = 16 \mu\text{s}$ ) (Barrington-Leigh & Inan, 1999; Newsome & Inan, 2010). These doublets were first thought to originate from the short rise time of the current waveform in the return stroke process (Marshall, 2012); however, the wide time separation between the peaks was later confirmed experimentally to correlate with high altitude compact intracloud lightning discharges (CIDs) (Lyu et al., 2015; Marshall et al., 2015). In 2017, elve “multiplets,” with more than two peaks in the photo trace, separated by much shorter time than previously observed, were anticipated to correlate with energetic in-cloud pulses (EIPs). EIPs were also believed to be responsible for the creation of particular terrestrial gamma ray flashes (TGFs) (Liu et al., 2017). These and other advances in detector sensitivity, including the facility described hereafter, and in lightning modeling suggest that multi-peaked elve measurements can be used to improve the understanding of the return stroke process in EIPs and CIDs, to study the link between elves and TGFs, and possibly, to provide insights into the initial breakdown (IB) processes (da Silva & Pasko, 2015; Marshall et al., 2014). Additionally, the study of single-peaked elves, known to be initiated by cloud-to-ground lightning, will help confirm the validity and limits of previously mentioned models at the most extreme lightning energies.

The Pierre Auger Observatory (Aab et al., 2015) was designed to measure ultrahigh energy cosmic rays (UHECR). As it turns out, the installed fluorescence detector (FD) (Abraham et al., 2010; Allekotte et al., 2008) has been observing elves since its debut in 2004 (Mussa & Ciaccio, 2012). The elves are observed above strong lightning strokes that lie below the horizon. Located on four different sites, FD telescopes point in fixed directions. As the field of view (FoV) of the telescopes overlap, the  $360^\circ$  azimuthal coverage of the detector is spanned more than once. The same elve may be measured by multiple FD telescopes, each with an optical aperture of 2.2-m diameter and a time resolution ( $\Delta\tau = 100 \text{ns}$ ) unprecedented in the field of TLE observations. The combination enables detailed measurements of large numbers of single-peaked and multi-peaked elves.

When a UHECR strikes the atmosphere, its kinetic energy is converted into an air shower of relativistic secondary particles, mostly electrons, positrons, and muons. These secondary particles collide inelastically with molecules in the troposphere, exciting the local nitrogen. The ultraviolet (UV) emission, also known as fluorescence, occurs from the fast de-excitation of  $\text{N}_2$  molecules, previously excited by low-energy ionization electrons left after the passage of the electromagnetic cascade in the troposphere (Arqueros et al., 2008; Rosado et al., 2014). The optics of the FD telescopes are optimized to capture the faint UV light arriving from the UHECR air shower development (Figure 1a). As for elves, the EMPs caused by the return strokes accelerate charged particles, primarily electrons, at the base of the ionosphere. The collisions between the particles and nitrogen molecule produce UV fluorescence light that is also observed by the FD (Figure 1b). Due to the fast radiative process of nitrogen in the UV (40 ns) (Valk et al., 2010), an elve measurement with a 100-ns time resolution is almost equivalent to a direct observation of the EMP. UHECR air showers are visible between about 3 and 30 km from a given FD site, depending on their energy. In contrast, the elves are much brighter due to the energy scale of lightning being much higher. The Auger Observatory has observed elves as far away as 1,500 km.

Using the fact that 95% of the observed elves are within 1,000 km from the Auger Observatory, which is beyond the distance where the axes of the lower pixels intercept a 92-km ionosphere, we can estimate the observational footprint of the Auger FD for elves to be  $3 \cdot 10^6 \text{ km}^2$ . This footprint covers portions of the Pacific Ocean, the Atlantic Ocean, Chile, the Andes mountain range, and Northern Argentina. The latter includes the Córdoba region, known for some of the most energetic and destructive convective thunderstorm systems

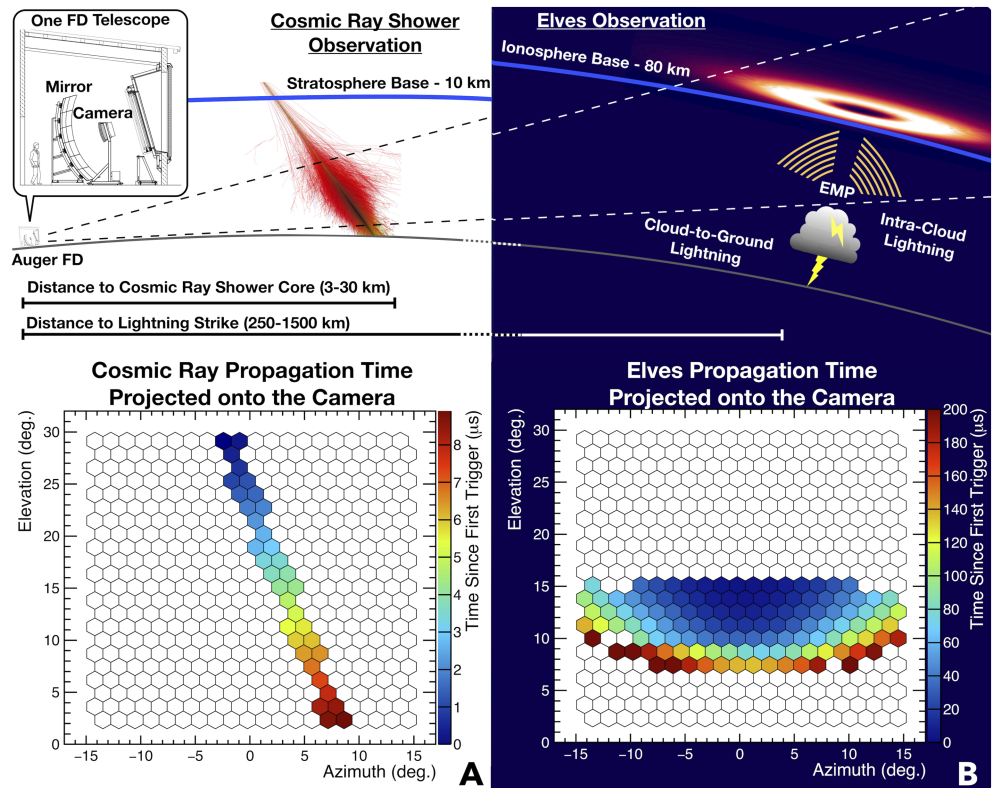


**Figure 1.** A diagram of the FD telescope with its 3.6 m diameter mirror at the Pierre Auger Observatory. The FD, optimized for the detection of cosmic rays up to 30 km, also turns out to be sensitive to elve signatures that are 1000 km away. The axes of the lowest pixels have an elevation angle of 1.5° while the axes of the highest pixels have elevation angles of 30°. (a) The time signature of a cosmic-ray shower propagating from top to bottom in the FoV of the Auger FD. (b) The first 200 μs of the propagation of an elve across an FD telescope camera FoV, showing the one side of the elves expanding towards the detector.

in the world (Rasmussen et al., 2014) and the highest lightning flash rate in some of the tallest thunderstorms (Zipser et al., 2006). The measurements of elves by the Auger Observatory, including many from this region of special interest, are expected to further the understanding of mechanisms that govern the production of the most intense lightning and to improve current models. The Auger Observatory will continue year-round operations, including observations of elves during dark night periods, until at least 2025.

In 2014, the FD readout and triggering algorithms were updated to better identify elve signatures and to record up to 300 μs of signal for each pixel of the camera. Hence, we report on 1,598 reconstructed, verified elves that were observed in the 3-year acquisition period, from 2014 to 2016. Using the unique capabilities of the FD, we sorted the data into two categories: 1,310 single-peaked and 288 multi-peaked elves. More extensive analysis of this data set will be published in future articles.

## 2. The Pierre Auger Observatory

The Auger Observatory measures the properties of the most energetic particles known to exist in the Universe and aims to discover their sources. The energy of a single “cosmic-ray” particle can reach  $10^{20}$  eV, an energy scale well beyond the reach of man-made accelerators. Ground-based cosmic-ray observatories are designed to detect secondary particles that are created when a high energy subatomic particle, from galactic or extragalactic origins, interacts with the atmosphere of the Earth. Cosmic rays collide with molecules in the troposphere or the lower stratosphere and create extended air showers, which the Auger Observatory measures using a surface array of 1,600 water-Cherenkov detectors (SD), spanning 3,000 km<sup>2</sup>, and a set of FDs (Abraham et al., 2010; Allekotte et al., 2008).

**Table 1**  
*Parameters of the Fluorescence Detector*

| Item                                    | Value        | Note                                     |
|---|--------------|--|
| Number of FD sites                      | 4            | Located on footprint outskirts           |
| Number of telescopes per site           | 6            | 180° azimuthal field of view             |
| Telescope optical aperture              | 2.2 m        | Extended diameter with corrector ring    |
| Field of view of one telescope          | 30° × 30°    | Azimuth × Elevation                      |
| Number of pixels per telescope          | 440          | Hexagonally shaped                       |
| Field of view of one pixel              | 1.5° × 1.5°  |  |
| Optical filter                          | Schott MUG-6 | Bandwidth: 300–420 nm, >680 nm           |
| Photomultiplier tube quantum efficiency | 30%          | 340–420 nm (0% above 700 nm)             |
| Time bin length                         | 100 ns       | Typically binned to 2 μs for long traces |
| Readout duration                        | 100–300 μs   | Including a 28-μs pedestal               |
| Absolute photometric calibration        | ±7%          |  |

We focus here on parameters of the FD (Table 1) that are important for the observation of elves. The FD telescopes (Figure 2a) point in fixed directions,  $\approx 17^\circ$  above the horizontal. The pointing directions, FoV, mirrors, UV optical filters, and photomultiplier tube cameras are optimized to measure the faint 300- to 400-nm light arriving from UHECR air showers through the troposphere. The quantum efficiency of the photomultiplier tubes is null above 700 nm, and the UV filter is opaque below 680 nm, limiting the detection of red and infrared light for all TLEs. Typical UHECR signals at the FD aperture are tens to thousands of photons/m<sup>2</sup>/100 ns, and typical viewing distances range from 3 to 30 km. In contrast, more than 95% of the observed elves are 250–1,000 km away, where the FoV of a telescope crosses the ionosphere and direct light from lightning is blocked by the limb of the Earth. In the signal observed at the FD, the higher intrinsic brightness of elves relative to the UHECRs compensates for the further distance to the elves. The tallest peak in the Andes mountain range may partly obstruct the last three rows of the telescopes pointing east, limiting the reconstruction of elve-inducing lightning beyond 1,000-km distances over the Pacific Ocean. The Auger FD operates on locally clear nights with low background from moonlight, accumulating about 1,200 hr of FD on-time over 12 months, equivalent to a 15% duty cycle. A suite of lasers, lidars, and IR cloud cameras measures the optical clarity of the atmosphere over the observatory (Aab et al., 2013a).

The FD telescopes are located at four sites. Six telescopes at each site are arranged for a total FoV of 180° (azimuth) × 30° (elevation). Due to the geometrical orientation of the FD sites, the physical aperture of the detector for the observation of elves is broken in three overlap regions: 8% seen by one site, 74% seen by

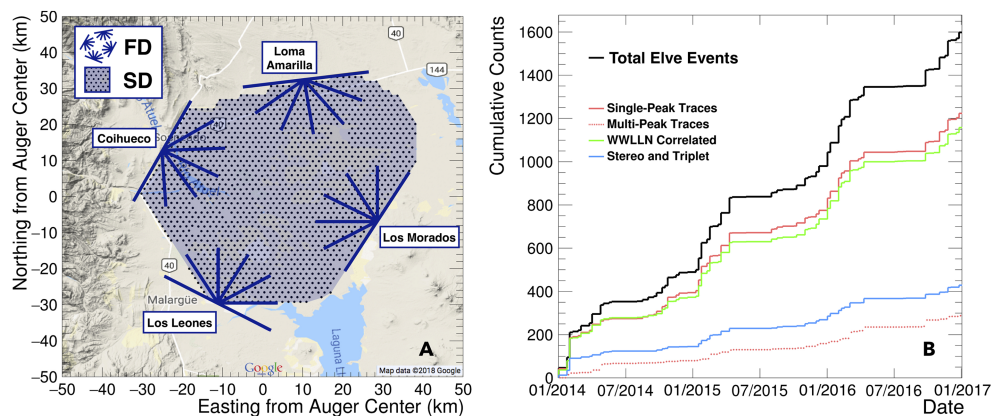


**Figure 2.** (a) The physical footprint of the Pierre Auger Cosmic-Ray Observatory is defined by the location of water-Cherenkov stations making up the surface detector (SD). The fluorescence detector (FD), used for the observation of elves, has a total of 24 telescopes positioned at four different sites on the outskirts of the SD. Six adjacent telescopes have a 180° field of view. (b) The cumulative elve data acquired by the Auger FD reached 1,598 counts in the 2014–2016 acquisition period. The count of elves with one peak in the photo traces is contrasted to the count of multip peaked elves. The number of Auger elves that are correlated to a WWLLN event within 5 ms is displayed in green.

two sites, and 18% seen by three sites. Detection probabilities due to variability in coverage are discussed in section 5.

The data readout of the Auger FD includes three trigger levels to select events of interest. The analog signals for each pixel are digitized every 100 ns and pass the first level trigger (FLT) if the analog-to-digital conversion (ADC) threshold requirement is satisfied. The second level trigger (SLT) is a pattern recognition designed to select UHECR signals; it requires at least four adjacent pixels passing the FLT. To form an event of interest and to be saved to disk, the traces have to pass the more complex third level trigger (TLT).

As part of the active interdisciplinary program pursued by the Auger Collaboration, we developed a TLT for lightning noise. Due to the time structure of the photo traces and the number of triggered pixels, these events are primarily detected by this lightning TLT. Then the events are searched for a radially expanding light front. Once the first triggered pixel is identified, pulse start times of the adjacent triggered pixels are required to have a monotonic growth. The trigger tolerates 20% of pixels that do not satisfy this cut. The algorithm requests at least three adjoining pixels to satisfy the described cut, on both sides of the first signal (only one side is required if the first pixel is close to the edge of a camera) and at least another three neighboring pixels above and below it.

### 3. Collected Data and Reconstruction of Lightning Location

The Pierre Auger Observatory started taking data in 2004. The fourth FD site, at Loma Amarilla, started operations in 2007. The first elve was observed in 2005, and two more events, which occurred in 2007, were discovered in a search for exotic events performed in 2009. A thorough search for elves in randomly saved events with loose trigger requirements, harvested in the period from 2007 to 2011, was exploited to design a modified TLT algorithm. The search yielded 58 more candidates (Aab et al., 2013b). In 2013, the observatory started acquiring elve candidates with the standard trace length (100  $\mu$ s), and in 2014, we improved the TLT to acquire up to 300  $\mu$ s of signal. In what follows, we present the data acquired during the 2014–2016 time period, for which we can now provide a more accurate reconstructed location and time. A seasonal dependence is present in the cumulative count of elves (Figure 2b). The three elongated flat regions correspond to the southern winter, June through August, when 43 elves were recorded over the course of 3 years. In contrast, we captured 711 elves over three summers. The discrete steps of the cumulative plot matched the nightly acquisition periods of the FD, as defined by the lunar cycle.

The first 28  $\mu$ s of the recorded traces occurred before the first photons from the emission region hit the detector and were used to calculate the baselines for each pixel; consequently, the true length of traces was 272  $\mu$ s. Because the FoV of individual FD sites overlap, we categorized elve candidates as mono (detected at one site), stereo (detected at two sites), or triplet (detected at three sites). We required that the same event was observed at all sites within 200  $\mu$ s. The raw data set consists of 2,311 elve candidates, including 1,864 mono, 396 stereo, and 51 triplet. To further increase the purity of the data sample, we verified that each candidate portrays the expected time structure and signal amplitude, and then we performed a geometric reconstruction.

With a 100-ns resolution, the FD distinguishes variations in the light emission caused by the internal structure of the EMP. Marshall (2012) and numerous others show quantitatively through analytics and numerics that the EMP created by cloud-to-ground (CG) lightning will structurally differ from an intracloud (IC) discharge. The ground is treated as a perfect conductor, which is a good approximation for very low frequency radiation of about 10 kHz. The physical process of the return stroke is trivialized to a current pulse traveling at a fraction of the speed of light along a wire (Rakov & Uman, 1998) and modeled as a Hertzian dipole, which is analytically solved using the method of images. We expect CG flashes, which are in contact with the ground, to radiate one large pulse directly toward the ionosphere. However, the IC flashes, not touching the conductor, would have the upper hemisphere of the dipole field radiate toward the ionosphere and the lower hemisphere of the dipole field radiate toward the ground. The downward propagating pulse bounces off the ground and travels behind the upward propagating pulse, reaching the ionosphere as a secondary pulse with a time delay related to the height of the lightning stroke. Due to the maximum height of clouds reaching about 17 km, we expect the presence of secondary pulses in the FD's photo traces, within 150  $\mu$ s from the primary pulses, to be a hint of IC lightning activity. More complex physics may also be a cause

of such structures. Selecting specific time decay constants of the current profile in the return stroke leads to substructure within the primary and secondary pulses (Liu et al., 2017). Initial breakdown (IB) pulses have been recorded within tens of microseconds from one another and could create multiple elves (da Silva & Pasko, 2015). Since multiple return strokes occur at the millisecond time scale and radiate significantly less energy, we do not interpret them as a cause of the internal structure observed in the Auger elve events. Finally, elves are distinctly different from other TLEs in the same vicinity to the ionosphere (sprites and halos). Sprites, mainly caused by the strong quasi-static fields of thunderstorms, would propagate vertically above the cloud and would not fit the geometry observed in the FD. On the other hand, sprite halos, also disk shaped and radially expanding, typically expand between 50 and 100 km and occur milliseconds after the stroke, while elves happen  $\approx 270 \mu\text{s}$  after the stroke (Miyasato et al., 2003). Compared to halos, almost all elves have a distinct hole in the center due to the shape of the dipole radiation, and they expand to radii greater than 200 km.

From the intrinsic time scale of the expanding elves, their varying locations, and the projected geometry at hand, we expected the amplitude, mean, and width of the observed traces to vary significantly depending on the pixel. When looking at pixels away from the first triggered pixel, the traces became wider and asymmetric. Also, the start time and amplitude of the pulses increased monotonically. A verification process, further described below, assessed whether candidates satisfied the expected trends: 1,727 of the candidate events were approved as elves, though not yet reconstructed.

In the verification process, we identified 1,403 single-peaked elves, suggesting that a cloud-to-ground (CG) lightning radiated the EMP. In Figure 3a, we show traces of a typical single-peaked elve event binned to  $2 \mu\text{s}$  to reduce the clutter in the plot. By recording the time of the peak maximum, we created the time propagation plot presented back in Figure 1b. We also integrated  $10 \mu\text{s}$  of the photo traces at relevant times to create snapshots of the signal in the telescope camera (Figure 3b). The arc-shaped signal correlated to a signal propagating up the camera, toward lower elevation angles. The cameras triggered on the outer most edge of the elve (disk shaped with  $\approx 250\text{-km}$  radius), closest to the observatory, and later acquired the signal above the lightning strike. The FD only recorded the half of the flash propagating toward the Auger Observatory. Patterns observed across all elve events are well featured in this example:

- The first pulse detected indicates the location of the shortest light propagation path to the lightning strike;
- the signal propagates down the rows with a rise in total photon count and pulse start time, until the hole above the lightning is reached;
- the lack of emission due to the dipole radiation pattern above the lightning strike is noticeable with the  $300\text{-}\mu\text{s}$  acquisition time used for the data set presented here;
- the amplitudes of the traces are strongly affected by the amount of atmosphere between the emission and the mirror; and
- the increased asymmetry of the pulses down the camera rows are a result of a wider observation area for pixels pointing at low elevation angles.

In addition to the single-peaked elves, we recognized 324 multi-peaked elves (18% of our data set), with trends in the traces that are similar to the single-peaked elves. Typical multi-peaked events have two distinct maxima; however, some events may have more than two distinguishable peaks. In Figures 3c and 3d, we present a typical double elve as observed by the Auger FD. In the first selected pixel (Pixel 1, in green), two peaks are separated by  $\approx 90 \mu\text{s}$ . To illustrate the FD resolution, we also display traces of an event with three clearly distinguishable peaks (Figures 3e and 3f). This structure is observed independently at two FD sites separated by 40 km, Coihueco and Loma Amarilla. In the first  $100 \mu\text{s}$ , the two telescopes recorded two peaks separated by  $\approx 20 \mu\text{s}$  in three selected pixels on the right of the camera. These two peaks may originate from IB discharges or more complex current profiles, as described previously. In the following  $100 \mu\text{s}$ , we are able to fit the third peak with the standard deviation of the first two combined. We interpret the third peak to be the bounces of the secondary pulses on the ground, distorted by the reflection and their projection on the ionosphere. In the case of an inclined dipole, we expect discrepancies in pulse amplitudes, often the case in IC discharge (Marshall et al., 2015).

We also performed a reconstruction of the location and time of the elve-inducing lightning. We first fitted the ADC trace for each pixel to an asymmetric Gaussian parametrized with the mean time, the signal amplitude, and the skewness, which related the left and right standard deviations:  $T_{\text{peak},i}$ ,  $A_{\text{peak},i}$ ,  $\sigma_{\text{left},i}$ , and  $\sigma_{\text{right},i} = \sigma_{\text{left},i} \cdot (1 + \delta)$ , where  $i$  is the index of the pixel. When dealing with multi-peaked elves, we selected the set of



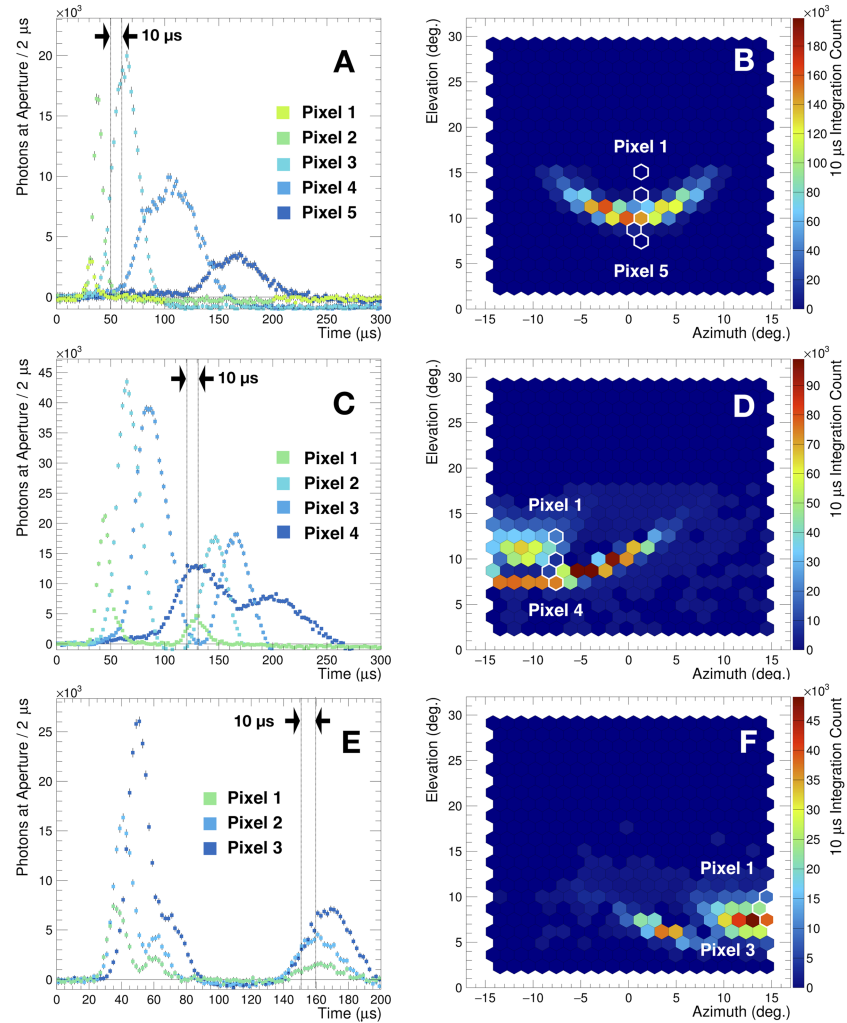


**Figure 3.** (a) Some 300- $\mu$ s-long traces of typical single-peaked elve observed in the FD at Los Leones, on 2 February 2014 at 05:12:22 UTC. (b) We selected 10  $\mu$ s of signal captured by the camera to show the arc shape of the elve. (c, d) Selected traces and a 10- $\mu$ s snapshot of a double-peaked event seen in Coihueco, on 17 January 2016 at 04:52:31 UTC. (e, f) 200- $\mu$ s-long traces and a 10- $\mu$ s snapshot of a multipeaked event seen in Los Leones, on 4 March 2016 at 05:32:39 UTC.

peaks ordered in time with the highest amplitude peak in the first triggered trace. Each pulse had to pass four quality criteria to be part of the reconstruction of the lighting location and time:

- $A_{\text{peak},i}$  greater than 300 ADC counts to select triggered pixels with sufficient signal,
- a relative error on  $A_{\text{peak},i}$  below 15% to disregard any traces with distorted profiles,
- $\sigma_{\text{left},i}(T)$  greater than 3  $\mu$ s to encompass the width of the trace in the first triggered pixel and all subsequent signals, and
- a relative error on  $\sigma_{\text{left},i}(T)$  below 25% to enforce the quality of the fit.

The parameters from the first fit were inputs to the second fit of the reconstruction, where we used a  $\chi^2$  minimization to obtain the time, latitude, longitude, and height ( $H_S$ ) of the lightning strike, and the height of the emission region at the base of the ionosphere ( $H_E$ ):

$$\chi^2 = \sum_{i=1}^{N_{\text{pix}}} (T_{\text{peak},i} - T_{\text{estimate},i})^2 / \sigma_i^2(T), \quad (1)$$

where  $T_{\text{estimate},i} = T_0 + \Delta T(\text{Lat}, \text{Lon}, H_E, H_S)$  was the estimated time at which light reached the detector after the propagation time,  $\Delta T$ , when added to the time of the lightning strike,  $T_0$ . We minimized the  $\chi^2$  by incrementally varying the position and time of the lightning, as well as the height of the ionosphere. The error on  $T_{\text{peak},i}$  came from the fit of the pixel trace. The model assumed that the EMP generated by the return

**Table 2**  
*Elves Counts Through Different Stages of the Analysis*

| Stage            | Mono  | Stereo | Triplet | Total | Note                            |
|------------------|-------|--------|---------|-------|---------------------------------|
| Triggered        | 1,864 | 396    | 51      | 2,311 | Independent of FD on-time       |
| Verified         | 1,287 | 390    | 50      | 1,727 | Features typical elve profile   |
| Confirmed        | 1,169 | 379    | 50      | 1,598 | Reconstructed at least one site |
| WWLLN correlated | 836   | 284    | 38      | 1,158 | 5-ms coincidence                |

*Note.* Each row is a subset of the one above.

stroke interacted in an infinitesimal layer at an atmospheric altitude  $H_E$ . The nitrogen fluorescence happens at negligible time scales ( $\approx 40$  ns, Valk et al., 2010) with respect to the total light propagation time from the strike to the detector, and with respect to the integration time of the camera.

In this paper, we present results with two constrained variables to reduce the complexity of the reconstruction. The fit allows Lat, Lon, and  $T_0$  to vary while fixing  $H_E$  at 92 km and  $H_S$  at the ground, even for multi-peaked elves. We base our guess of the ionosphere height on our timing correlation with World Wide Lightning Location Network (WWLLN) (presented in the next section), a few kilometers higher in altitude than observations made in South-Western Europe (van der Velde & Montanyà, 2016). The South Atlantic Anomaly may be a factor affecting the altitude of the ionosphere base.

Ultimately, we may have observed an event at more than one FD site but reconstructed it solely once. Hence, we define a *confirmed* elve event as one that passed the verification stage and that was reconstructed at least once. In this 3-year data set, we found 1,598 confirmed elve flashes. In addition, the coverage of WWLLN in Argentina is such that three antennas are within the observational footprint for elves of the Auger FD (Hutchins et al., 2012; Jacobson et al., 2006). Our correlation with the network was 72%: 1,158 Auger elves correlated within 5 ms of a WWLLN reconstructed lightning strike. A finer time correlation study will be presented in the next section. We summarize all event counts in Table 2.

#### 4. Time Correlation, Energy Distribution, and Spatial Resolution

To refine the timing correlation with WWLLN, we estimate the shortest propagation time of light from the lightning strike reconstructed by WWLLN to the ionosphere and finally to the FD detector. For most elves, we suggest that the point on the ionosphere, halfway between the lightning strike and the FD, is where the first detected light emission would occur. Any elve not large enough to reach that halfway point has an underestimated time of the lightning strike. If the height of the ionosphere is not well chosen, then all time estimates are also miscalculated. After adding the calculated propagation time to the WWLLN reconstructed strike time, assumed to be at the ground, we compare the result to the Auger FD trigger time (Figure 4a, blue curve). The mean of the distribution is sensitive to the height of the infinitesimal ionospheric layer, where the emission is assumed to originate. If the ionosphere height is overestimated, light traveled a longer distance to reach the detector, and we overestimate the time at which the first photons reached the FD. A 92-km ionosphere base has almost no offset on the position of the mean,  $\mu_{\text{WWLLN}} = 2 \pm 1 \mu\text{s}$ , while an 85-km height wrongly overestimates our trigger time by  $20 \pm 1 \mu\text{s}$  and a 100-km height underestimates it by  $19 \pm 1 \mu\text{s}$ . The WWLLN resolution in the Auger FoV drives the distribution width of  $28 \mu\text{s}$  ( $\approx 8$  km).

The reconstruction of elves provides an estimate of the lightning strike time based on the fitted location as measured at individual FD sites. We detailed this process in section 3. Comparing the results obtained at any two FD sites observing the same event, using 363 stereo and triplet events with all triggered sites reconstructed, yields an estimate of our reconstruction timing resolution (Figure 4a, red curve). The 39- $\mu\text{s}$  RMS indicates an FD mono resolution ( $\sigma_{\text{mono}} = \sigma_{\text{stereo}}/\sqrt{2}$ ) of  $28 \mu\text{s}$  ( $\approx 8$  km). Hence, at first glance, our reconstruction is doing as well as the reconstruction of WWLLN at timing the lightning strike. Finally, we compare directly the Auger reconstruction and the WWLLN reconstruction (Figure 4a, black curve). The standard deviation of the black curve is more than the Auger mono contribution and the WWLLN contribution added in quadrature; hence, there is 5–10  $\mu\text{s}$  of unknown systematics. With the current status of the reconstruction, we are able to almost match WWLLN in locating the lightning strikes, but we slightly overestimate the time at which the events happened. Both the WWLLN and the Auger reconstructions use signal traces as fundamental inputs. We do not know what part of the trace was used as the start time in

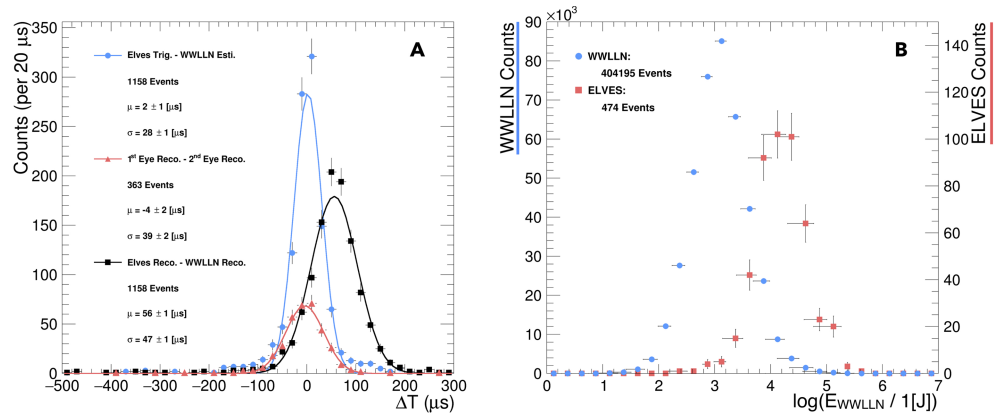


**Figure 4.** (a) The timing correlation between the reconstructed lighting strike of WWLLN, added to the shortest propagation time from the strike location to the Auger FD, and triggered time stamp in the FD, shown in red. The difference between two independent reconstructions of the same elve observed at two FD sites is shown in blue. (b) Comparison between the distribution of lightning energy for all WWLLN events measured in the FoV of the active FD and those WWLLN events correlated to elves measured by Auger, from 2014 through 2016.

the WWLLN reconstruction, which could contribute significantly to the offset observed in the black curve. Possible sources of error to explore are the differentiation between IC and CG sources in the WWLLN data set, as well as in the elve data set. Two additional parameters in the Auger reconstruction will be released for multi-peaked events to improve the timing resolution. In addition, elves are created from an EMP with a wider frequency band and a greater energy density than the EMP observed by WWLLN; hence, we expect our photo traces to differ from the direct observation of that network.

By applying a cut on the distance from the Auger Observatory on both the Auger elves and the WWLLN lightning strike (250 to 1,000 km still selecting >95% of observed elves) and requiring all FD sites to be active (in data taking mode), we compare the energy of lightning which created elves to that of all lightning observed by WWLLN within this time and footprint (Figure 4b). This distance cut is chosen to optimize the comparison between events of both data sets happening within the FoV of the Auger FD. WWLLN records the far-field radiated electromagnetic energy in the 6- to 18-kHz frequency band. The peak radiated energy is known to be in the 10- to 15-kHz range. The 474 confirmed elve events satisfying the above correlation requirements are correlated to WWLLN events at the high end of the energy spectrum. We omitted elves with more than one WWLLN event correlated within the 5-ms coincidence. Adding those events to the analysis uniformly increases the counts in the last four bins. To obtain the median energy of both data sets, we calculate the mean of the log-normal distributions to obtain  $16 \pm 2$  kJ for the matched elves and  $1.3 \pm 0.1$  kJ for all lightning. Using an empirical equation for peak current (Hutchins et al., 2012),

$$I_0 = (E_{\text{WWLLN}} / (1.3 \cdot 10^{-3} \cdot 1,676))^{0.6173}, \quad (2)$$

where  $E_{\text{WWLLN}}$  is the recorded far-field radiation energy in Joule; the calculated median energy for the 404,195 selected WWLLN lightning strikes converts to a median peak current of  $51 \pm 3$  kA. Equation (2) was obtained on low- to middle-energy lightning strikes. Because this range does not have a strong overlap with the 474 strikes matched to the Auger elve data, we do not provide a peak current for these strikes.

To illustrate the spatial resolution of the reconstructed lightning location obtained from elves, we transform from geodetic coordinates to a local Auger coordinate system. This transformation provides the reconstructed distance and azimuth of the lightning. In Figures 5a and 5b, we present the difference between the reconstructed lightning locations of WWLLN and Auger, with respect to the location of the Auger FD. For comparison, we also provide the reconstructed lightning locations by the Auger Observatory for elves observed in stereo (Figures 5c and 5d). For all the plots, the analysis requires more than 10 events in every 50-km bin for the calculation of a mean and RMS. The lighter color indicates the RMS in each bin, while the darker color portrays the statistical error on the mean. The uncertainties of both the WWLLN and Auger reconstructions contribute to the error of the blue plots. The current reconstruction of elves systematically overestimates the distance of the lightning strike by 15 km. This consistent offset as a function of distance

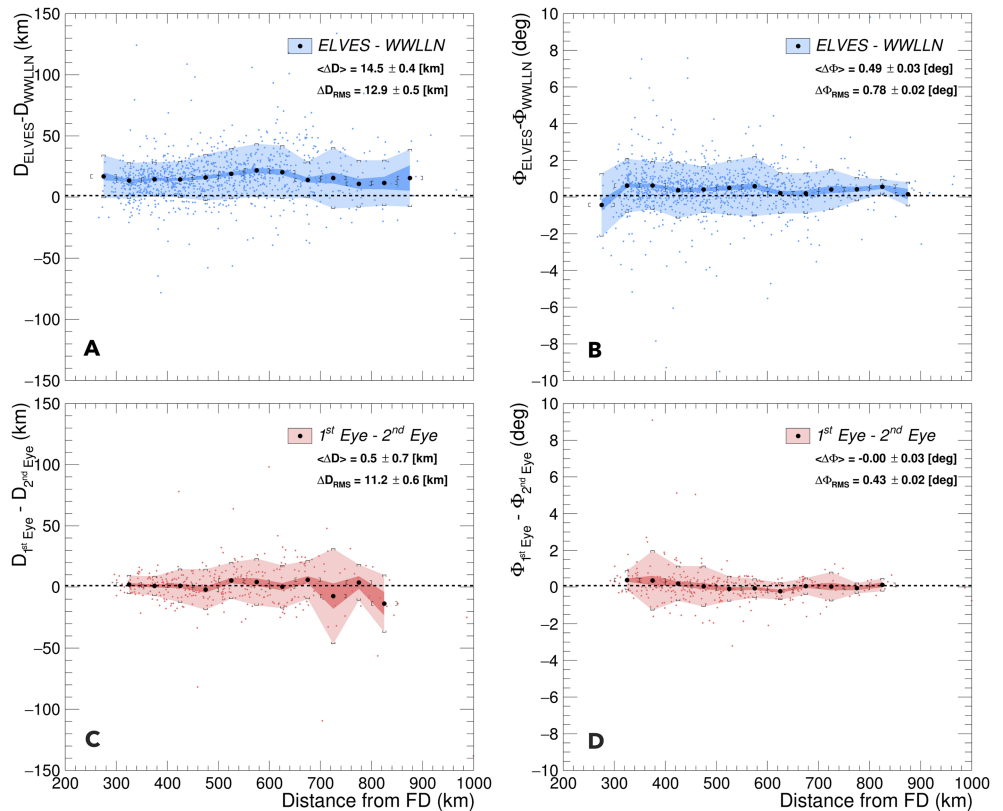


**Figure 5.** We present an assessment of the Auger reconstruction quality performed by converting all geodetic locations to a distance,  $D$ , and an azimuth,  $\Phi$ , with respect to the observing FD site. The distance is the lightning strike distance from the triggered FD site, while the angle is the azimuth due east. (a, b) We compare the lightning strike location reconstructed by WWLLN to the location reconstructed from the observation of the elve. (c, d) We test the position resolution between two Auger reconstructions of a stereo or triplet observation.

from the Auger Observatory is compatible with the timing observed in Figure 4, hinting at a discrepancy between signal start times of Auger elves and WWLLN far-field radiation measurements. The combined RMS of the distance and azimuth difference plots also agrees with the timing resolution.

### 5. Lightning Location Maps

To disentangle dense elve regions from high observation probability regions, we display the reconstructed location of the elve-inducing lightning in four Mercator projected, high-resolution maps (Figure 6). More than 90% of the elves detected by the Auger Observatory are to the east of the detector center (lat. =  $-35.25^\circ$ , lon. =  $-69.25^\circ$ ). In contrast, we confirm only six events to the west of the Andes mountain chain. Two blue circles define the FD FoV projected onto a plane at 92-km altitude: the inner circle coincides with the upper edge of the pixels at  $30^\circ$  elevation from the ground, while the outer circle bounds the lower edge of the pixels at  $1.5^\circ$  elevation. These inner and outer contours are at 110 and 860 km from the center of the Auger Observatory, respectively. Multiple FD sites observing in the same region have a higher chance of an elve observation. We aim at disentangling our high detection probability in the north-east from the high occurrence of elves in that region.

Each data point in the maps is the location of the lightning strike reconstructed from an elve. The inhomogeneous strike density, as a function of distance from the center of the Auger Observatory, reveals unavoidable cutoffs for data acquisition in the observational footprint of the FD. When too close to the horizon, the light from the top of thunderstorm systems may reach the pixel array before the light emission from the ionosphere. The discarded lightning events induce a natural inner cutoff at  $\approx 230$  km.

We color the overlap regions of the detector FoV in green for mono, blue for stereo, and orange for triplet (Figure 6a). As an overlay, we plot the location of the center of the elve (i.e., the reconstructed lightning

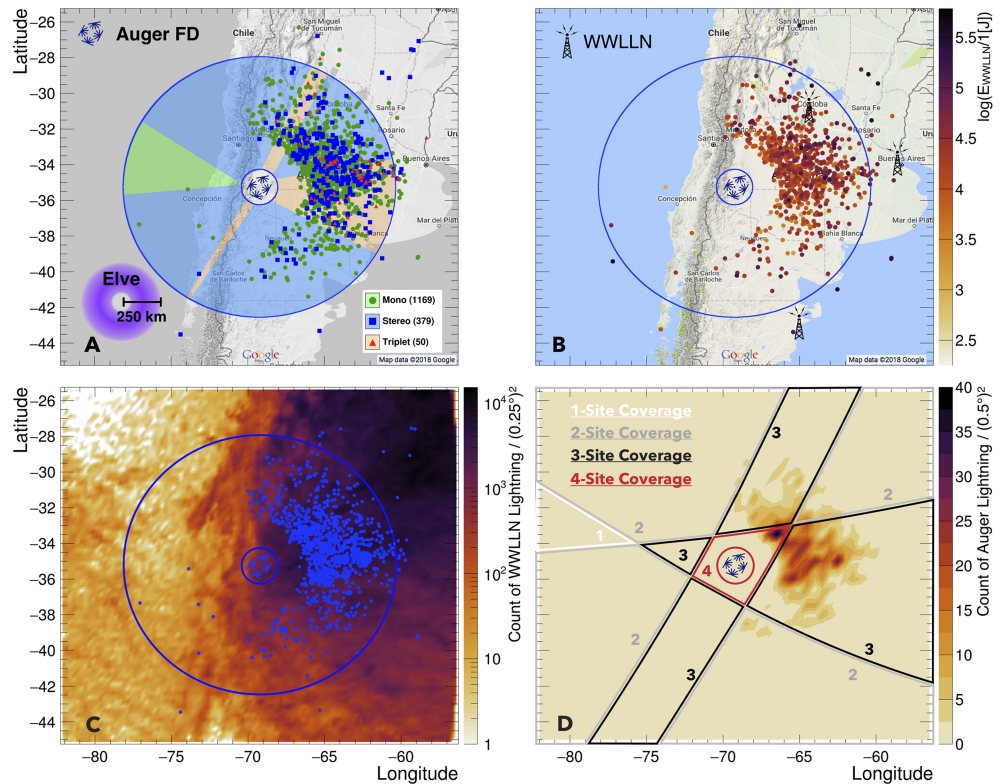


**Figure 6.** These maps denote the location of the reconstructed lightning strikes causing elves seen by the observatory, in geodetic coordinates. The large and small circles outline the lower and upper boundaries of the pixel array when projected to the base of the ionosphere, approximately with 860 and 110-km radius, respectively. (a) The reconstructed lightning strike location from Auger elves and the number of FD sites contributing to each observation. The overlap of the FoV of each FD sites is shown in the shaded regions. (b) The WWLLN events correlated with our elve data set against a log-color scale representing their energy in Joule. (c) A density map of WWLLN events with an overlay of elve-inducing lightning in coincidence. (d) The one-site, two-site, three-site, and four-site coverage regions as an overlay on a density map of reconstructed locations of lightning strikes obtained from Auger elves.

location) based on their observation duplicity. In the mono region, the FD recorded only one event despite the 1,172 events observed only by one site in the rest of the FoV. Because the size of an elve, as defined by its UV emission region, spans a few hundred kilometers, we reconstructed 17 of the 50 triplet events outside a triplet overlap region. The proportionality of triplet events to mono and stereo events indicates a detection inefficiency induced by factors such as the trigger algorithms, the detector on-times, the reconstruction, and other phenomenological effects such as clouds between the light emission and an FD site.

From the energy map of WWLLN events matched in time to Auger elves, we observe that the FD tends to trigger on higher energy events when the lightning location is outside the physical, projected aperture (Figure 6b). At closer distances, the FoV overlap located east of the Auger Observatory increases the observation probability, and the light from the emission region travels through less atmosphere to reach the telescopes. Hence, the Auger FD triggers on numerous, dimmer events at near distances.

By cross-checking the on-time of the Auger FD with the WWLLN data set, we created a density map of WWLLN lightning events displayed on a log scale with quarter geodetic degree bin size (Figure 6c). From this heat map of WWLLN events acquired from 2014 to 2016, uncorrected for relative detection inefficiencies (Hutchins et al., 2012), we confirm the high density of lightning strikes present in the north-east of Argentina. The low density of lightning strikes over the ocean coincides with the low elve count observed by the Auger Observatory, consistent with the lightning climatology study of Virts et al. (2013). In this map, we do not require an energy value from WWLLN as a selection for the elve events, but only a 5-ms timing coincidence.

To confirm the anisotropic elve distribution, we investigate the increased probability of observation in the surrounding overlap regions. Assuming a hypothetical flat elve at 92-km altitude, with an averaged radius of 250 km and an equal detection probability at all FD sites, we calculate the percentage of that elve in the FoV of each sites. The value for the elve radius is representative of the Auger data set; it is much larger than what was previously reported by the PIPER experiment (Blaes et al., 2014). If at least 15% of the elve is in the FoV of an FD site, then we flag the center of that elve as a geodetic location with elve-inducing lightning, detectable by the Auger Observatory. From the number of FD sites which can detect at least 15% of the same elve, we infer coverage regions which differed from the overlap regions mentioned previously (Figure 6d): one-site, two-site, three-site, and four-site coverage. If lightning strikes in a three-site coverage region, three FD sites will have at least 15% of the hypothetical elve in their FoV. This map of expected coverage configurations indicates the presence of a four-site coverage region. If a 500-km-diameter elve is centered around a geodetic location in that four-site coverage region, it covers two different triplet overlap regions. This map also suggests an expanded region for possible triplet observations, where the probability to make an observation in that three-site region ( $P = 1 - (1 - \epsilon)^3$ , with  $\epsilon$  representing the detection probability for one site), is greater than the probability of an observation in a two-site region ( $P = 1 - (1 - \epsilon)^2$ ). A superposition of the coverage with a heat map of the Auger reconstructed lightning location data explains the hot spot in the four-site region ( $P = 1 - (1 - \epsilon)^4$ ), at geodetic coordinates ( $-33.5^\circ, -66.5^\circ$ ).

We obtain an estimate for the probability from the lack of triplet observation in a three-site coverage region, where most of the events occurred in this 3-year data set. The ratio of mono to stereo counts, mono to triplet counts, or stereo to triplet counts is correlated, through basic probability theory, to an estimate of the observation probability for a single site of  $35 \pm 8\%$ . Consequently, we calculate the probability to detect an elve by using the simple formulas mentioned previously, to be  $82 \pm 9\%$  for an elve-inducing lightning in a four-site coverage region ( $73 \pm 10\%$  in a three-site region); however, this detection inefficiency leads to a probability of making a quadruplet observation ( $\epsilon^4$ ) closer to one in a hundred. With another few years of data, we anticipate the detection of an elve with all FD sites. Multiple-site observations also become a useful tool to understand the atmospheric attenuation and confirm the total amount of photons emitted at the base of the ionosphere. With the analysis described here, we will track the changes in our efficiencies after each improvement of the trigger algorithm. Ultimately, we will be able to obtain a number for the minimum lightning energy needed to create elves in our FoV.

## 6. Summary

After adding a new trigger channel to target a class of atmospheric TLEs known as elves, the Pierre Auger Observatory has recorded almost 1,600 of these events over the 3-year period from 2014 to 2016. This cosmic-ray observatory, located in the Mendoza province of Argentina, includes 24 fixed-direction UV fluorescence photometric telescopes distributed over four different sites. These telescopes operate every night when the weather is reasonably clear and the moonlight is sufficiently low. The total FoV of the FD spans in azimuth the entire horizon, and 92% of it is covered by two FD sites. Several hundred photomultiplier pixels, digitized at 10 MHz, participate in a typical elve measurement. The data set reported here demonstrates that the observatory acceptance for elves extends over  $3 \cdot 10^6 \text{ km}^2$ .

We developed an algorithm to reconstruct the latitude and longitude of the lightning from the measured light-time distributions of the recorded elves. A list of the coordinates, and UTC times, of 1,598 elves is available on the website of the Pierre Auger Observatory. When the height of the UV emission is constrained to 92 km above sea level, the current state of the resolution analysis shows that we agree with a WWLLN estimate of the FD trigger time. This analysis also shows that we slightly overestimate the distance and time of our reconstructed events; 72% of the observed elves correlate with independent radio-frequency measurements of lightning by WWLLN. For a quality subset of these correlated events (474), the lightning energy as measured by WWLLN had a median of 16 kJ, while the median energy of all lightning measured by WWLLN that occurred inside the elve footprint while the telescopes were taking data was 1.3 kJ. Using this particular lightning data set and lightning energies, the turn-on threshold for elve detection by the Auger Observatory is about an order of magnitude higher than the turn-on threshold for lightning detection by WWLLN.

The observed elve locations exhibited seasonal and geographical patterns: 44% of the elves observed occurred during the southern-summer months, and just 2.5% occurred during winter months. Nearly all of the

**Acknowledgments**

The time and location of the 1,598 verified and reconstructed elves, used for the analysis showcased in this paper, are publicly available on the website of the Pierre Auger Observatory (<https://www.auger.org/index.php/science/data>). We wish to thank the World Wide Lightning Location Network (<http://wwlln.net>), a collaboration among over 50 universities and institutions, for providing the lightning location data used in this paper. We acknowledge Robert Marshall for providing one of the most advanced elve simulations to the public, a key tool in understanding the elves observed by the Pierre Auger Observatory. The successful installation, commissioning, and operation of the Pierre Auger Observatory would not have been possible without the strong commitment and effort from the technical and administrative staff in Malargüe. We are very grateful to the following agencies and organizations for financial support: Argentina—Comisión Nacional de Energía Atómica; Agencia Nacional de Promoción Científica y Tecnológica (ANPCyT); Consejo Nacional de Investigaciones Científicas y Técnicas (CONICET); Gobierno de la Provincia de Mendoza; Municipalidad de Malargüe; and NDM Holdings and Valle Las Leñas, in gratitude for their continuing cooperation over land access; Australia—the Australian Research Council; Brazil—Conselho Nacional de Desenvolvimento Científico e Tecnológico (CNPq); Financiadora de Estudos e Projetos (FINEP); Fundação de Amparo à Pesquisa do Estado de Rio de Janeiro (FAPERJ); São Paulo Research Foundation (FAPESP) Grants 2010/07359-6 and 1999/05404-3; Ministério da Ciência, Tecnologia, Inovações e Comunicações (MCTIC); Czech Republic—Grants MSMT CRLTT18004, LO1305, LM2015038, and CZ.02.1.01/0.0/0.0/16\_013/0001402; France—Centre de Calcul IN2P3/CNRS; Centre National de la Recherche Scientifique (CNRS); Conseil Régional Ile-de-France; Département Physique Nucléaire et Corpusculaire (PNC-IN2P3/CNRS); Département Sciences de l’Univers (SDU-INSU/CNRS); Institut Lagrange de Paris (ILP) Grant LABEX ANR-10-LABX-63 within the Investissements d’Avenir Programme Grant ANR-11-IDEX-0004-02; Germany—Bundesministerium für Bildung und Forschung (BMBF); Deutsche Forschungsgemeinschaft (DFG); Finanzministerium Baden-Württemberg; Helmholtz Alliance for Astroparticle Physics (HAP); Helmholtz-Gemeinschaft

observed elves appeared east of the Andes, and just two were observed and reconstructed over the Pacific Ocean, confirming a study by Virts et al. From the multiplicity of peaks in the traces, we conclude that 18% of our data set was related to IC lightning activity (at least two peaks in the photo trace) while the rest shows simpler structure.

The Pierre Auger Observatory is scheduled to operate until at least 2025. In 2017, we implemented a deeper readout window of 900 μs for elves, to increase the quality of our current reconstruction. We are planning refinements of the on-line TLE-trigger algorithm. To our knowledge, the Auger Observatory is the first and only ground-based facility that measures elves with year-round operation with full horizon coverage, controlled photon counting, and 100-ns resolution. We look forward to possible correlation studies between Auger data and various ongoing experiments: the RELAMPAGO ground-based lightning detection campaign (Nesbitt et al., 2017), the GLM instrument aboard the GOES-16 satellite (Goodman et al., 2013), the ASIM TLE detector (Neubert et al., 2009) and the Mini-EUSO cosmic-ray detector (Capel et al., 2018) aboard the space station, the TARANIS satellite (Lefevre et al., 2008), and private ground-based networks such as the GLD-360 of Vaisala, Inc (Demetriades, 2012) or the ENTLN of Earth Networks (Heckman, 2014). Any correlation analysis would contribute significantly to atmospheric electricity research.

**Acronyms**

|                |  |
|----------------|--|
| <b>TLE</b>     | transient luminous event   |
| <b>elve(s)</b> | Emission of Light from Very low frequency perturbations due to Electromagnetic pulse Sources |
| <b>FD</b>      | fluorescence detector  |
| <b>SD</b>      | surface detector   |
| <b>CCD</b>     | charge-coupled device  |
| <b>ISUAL</b>   | Imager of Sprites and Upper Atmospheric Lightning  |
| <b>PIPER</b>   | Photometric Imager of Precipitated Electron Radiation  |
| <b>CG</b>      | cloud-to-ground  |
| <b>IC</b>      | intracloud   |
| <b>EIP</b>     | energetic IC pulses  |
| <b>CID</b>     | compact IC discharges  |
| <b>UHECR</b>   | ultrahigh energy cosmic rays   |
| <b>UV</b>      | ultraviolet  |
| <b>EMP</b>     | electromagnetic pulse  |
| <b>WWLLN</b>   | World Wide Lightning Location Network  |
| <b>TLT</b>     | third level trigger  |
| <b>SLT</b>     | second level trigger   |
| <b>FLT</b>     | first level trigger  |
| <b>FoV</b>     | field of view  |
| <b>IB</b>      | initial breakdown  |
| <b>ADC</b>     | analog-to-digital converter  |

**References**

Aab, A., et al. (2013a). Techniques for measuring aerosol attenuation using the Central Laser Facility at the Pierre Auger Observatory. *Journal of Instrumentation*, 8(4), P04009. <http://stacks.iop.org/1748-0221/8/i=04/a=P04009>

Aab, A., et al. (2013b). The Pierre Auger Observatory: Contributions to the 33rd International Cosmic Ray Conference (ICRC 2013). <http://arxiv.org/abs/1307.5059>

Aab, A., et al. (2015). The Pierre Auger Cosmic Ray Observatory. *Nuclear Instruments and Methods in Physics Research, Section A: Accelerators, Spectrometers, Detectors and Associated Equipment*, 798, 172–213. <https://doi.org/10.1016/j.nima.2015.06.058>

Abraham, J., et al. (2010). The fluorescence detector of the Pierre Auger Observatory. *Nuclear Instruments and Methods in Physics Research Section A: Accelerators, Spectrometers, Detectors and Associated Equipment*, 620(2-3), 227–251. <https://doi.org/10.1016/J.NIMA.2010.04.023>

Allekotte, I., Barbosa, A. F., Bauleo, P., Bonifazi, C., Civit, B., Escobar, C. O., et al. (2008). The surface detector system of the Pierre Auger Observatory. *Nuclear Instruments and Methods in Physics Research Section A: Accelerators, Spectrometers, Detectors and Associated Equipment*, 586(3), 409–420. <https://doi.org/10.1016/J.NIMA.2007.12.016>

Arqueros, F., Hörandel, J. R., & Keilhauer, B. (2008). Air fluorescence relevant for cosmic-ray detection—Summary of the 5th fluorescence workshop, El Escorial 2007. *Nuclear Instruments and Methods in Physics Research Section A: Accelerators, Spectrometers, Detectors and Associated Equipment*, 597(1), 1–22. <https://doi.org/10.1016/j.nima.2008.08.056>

Baba, Y., & Rakov, V. A. (2007). Electromagnetic models of the lightning return stroke. *Journal of Geophysical Research*, 112, D04102. <https://doi.org/10.1029/2006JD007222>

- Deutscher Forschungszentren (HGF); Ministerium für Innovation, Wissenschaft und Forschung des Landes Nordrhein-Westfalen; Ministerium für Wissenschaft, Forschung und Kunst des Landes Baden-Württemberg; Italy—Istituto Nazionale di Fisica Nucleare (INFN); Istituto Nazionale di Astrofisica (INAF); Ministero dell'Istruzione, dell'Università e della Ricerca (MIUR); CETEMPS Center of Excellence; Ministero degli Affari Esteri (MAE); México—Consejo Nacional de Ciencia y Tecnología (CONACYT)167733; Universidad Nacional Autónoma de México (UNAM); PAPIIT DGAPA-UNAM; The Netherlands—Ministry of Education, Culture and Science; Netherlands Organisation for Scientific Research (NWO); Dutch National e-Infrastructure with the support of SURF Cooperative; Poland—National Centre for Research and Development, Grant ERA-NET-ASPERA/02/11; National Science Centre, Grants 2013/08/M/ST9/00322, 2016/23/B/ST9/01635, and HARMONIA 5–2013/10/M/ST9/00062, UMO-2016/22/M/ST9/00198; Portugal—Portuguese national funds and FEDER funds within Programa Operacional Factores de Competitividade through Fundação para a Ciência e a Tecnologia (COMPETE); Romania—Romanian Ministry of Research and InnovationCNCS/CCDI-UESFISCDI, projects PN-III-P1-1.2-PCDDI-2017-0839/19PCDDI/2018, PN-III-P2-2.1-PED-2016-1922, PN-III-P2-2.1-PED-2016-1659, and PN18090102 within PNCDI III; Slovenia—Slovenian Research Agency; Spain—Comunidad de Madrid; Fondo Europeo de Desarrollo Regional (FEDER) funds; Ministerio de Economía y Competitividad; Xunta de Galicia; European Community 7th Framework Program Grant FP7-PEOPLE-2012-IEF-328826; USA—Department of Energy, Contracts DE-AC02-07CH11359, DE-FR02-04ER41300, DE-FG02-99ER41107, and DE-SC0011689; National Science Foundation, Grant 0450696; The Grainger Foundation; Marie Curie-IRSES/EPLANET; European Particle Physics Latin American Network; European Union 7th Framework Program, Grant PIRSES-2009-GA-246806; and UNESCO.
- Barrington-Leigh, C. P., & Inan, U. S. (1999). Elves triggered by positive and negative lightning discharges. *Geophysical Research Letters*, *26*, 683–686.
- Blaes, P. R., Marshall, R. A., & Inan, U. S. (2014). Return stroke speed of cloud-to-ground lightning estimated from elve hole radii. *Geophysical Research Letters*, *41*, 9182–9187. <https://doi.org/10.1002/2014GL062392>
- Boeck, W. L., Vaughan, O. H., Blakeslee, R., Vonnegut, B., & Brook, M. (1992). Lightning induced brightening in the airglow layer. *Geophysical Research Letters*, *19*(2), 99–102. <https://doi.org/10.1029/91GL03168>
- Capel, F., Belov, A., Casolino, M., & Klimov, P. (2018). Mini-EUSO: A high resolution detector for the study of terrestrial and cosmic UV emission from the International Space Station. *Advances in Space Research*, *62*(10), 2954–2965. <https://doi.org/10.1016/J.ASR.2017.08.030>
- Chen, A. B., Kuo, C., Lee, Y., Su, H., Hsu, R., Chern, J., et al. (2008). Global distributions and occurrence rates of transient luminous events. *Journal of Geophysical Research*, *113*, A08306. <https://doi.org/10.1029/2008JA013101>
- Chern, J. L., Hsu, R. R., Su, H. T., Mende, S. B., Fukunishi, H., Takahashi, Y., & Lee, L. C. (2003). Global survey of upper atmospheric transient luminous events on the ROCSAT-2 satellite. *Journal of Atmospheric and Solar-Terrestrial Physics*, *65*(5), 647–659. [https://doi.org/10.1016/S1364-6826\(02\)00317-6](https://doi.org/10.1016/S1364-6826(02)00317-6)
- Cho, M., & Rycroft, M. J. (2001). Non-uniform ionisation of the upper atmosphere due to the electromagnetic pulse from a horizontal lightning discharge. *Journal of Atmospheric and Solar-Terrestrial Physics*, *63*(6), 559–580. [https://doi.org/10.1016/S1364-6826\(00\)00235-2](https://doi.org/10.1016/S1364-6826(00)00235-2)
- da Silva, C. L., & Pasko, V. P. (2015). Physical mechanism of initial breakdown pulses and narrow bipolar events in lightning discharge. *Journal of Geophysical Research: Atmospheres*, *120*, 4989–5009. <https://doi.org/10.1002/2015JD023209>
- Demetriades, N. (2012). Advanced lightning warning systems are now available worldwide, Meteorological Technology International.
- Fukunishi, H., Takahashi, Y., Kubota, M., Sakanoi, K., Inan, U. S., & Lyons, W. A. (1996). Elves: Lightning-induced transient luminous events in the lower ionosphere. *Geophysical Research Letters*, *23*(16), 2157–2160. <https://doi.org/10.1029/96GL01979>
- Goodman, S. J., Blakeslee, R. J., Koshak, W. J., Mach, D., Bailey, J., Buechler, D., et al. (2013). The GOES-R Geostationary Lightning Mapper (GLM). *Atmospheric Research*, *125–126*, 34–49. <https://doi.org/10.1016/J.ATMOSRES.2013.01.006>
- Heckman, S. (2014). ENTLN status update. In *XV International Conference on Atmospheric Electricity*. Norman, OK: National Weather Service.
- Hutchins, M. L., Holzworth, R. H., Brundell, J. B., & Rodger, C. J. (2012). Relative detection efficiency of the World Wide Lightning Location Network. *Radio Science*, *47*, RS6005. <https://doi.org/10.1029/2012RS005049>
- Hutchins, M. L., Holzworth, R. H., Rodger, C. J., & Brundell, J. B. (2012). Far-field power of lightning strokes as measured by the World Wide Lightning Location Network. *Journal of Atmospheric and Oceanic Technology*, *29*(8), 1102–1110. <https://doi.org/10.1175/jtech-d-11-00174.1>
- Inan, U. S., Barrington-Leigh, C., Hansen, S., Glukhov, V. S., Bell, T. F., & Rairden, R. (1997). Rapid lateral expansion of optical luminosity in lightning-induced ionospheric flashes referred to as 'elves'. *Geophysical Research Letters*, *24*(5), 583–586. <https://doi.org/10.1029/97GL00404>
- Inan, U. S., Bell, T. F., & Rodriguez, J. V. (1991). Heating and ionization of the lower ionosphere by lightning. *Geophysical Research Letters*, *18*(4), 705–708.
- Jacobson, A. R., Holzworth, R., Harlin, J., Dowden, R., & Lay, E. (2006). Performance assessment of the World Wide Lightning Location Network (WWLLN), using the Los Alamos Sferic Array (LASA) as ground truth. *Journal of Atmospheric and Oceanic Technology*, *23*(8), 1082–1092. <https://doi.org/10.1175/JTECH1902.1>
- Lefevre, F., Blanc, E., Pinçon, J.-L., Roussel-Dupré, R., Lawrence, D., Rauch, J.-L., et al. (2008). TARANIS—A satellite project dedicated to the physics of TLEs and TGFs. *Space Science Reviews*, *137*(1–4), 301–315. <https://doi.org/10.1007/s11214-008-9414-4>
- Liu, N., Dwyer, J. R., & Cummer, S. A. (2017). Elves accompanying terrestrial gamma ray flashes. *Journal of Geophysical Research: Space Physics*, *122*, 10,510–563,576. <https://doi.org/10.1002/2017JA024344>
- Lyu, F., Cummer, S. A., & McTague, L. (2015). Insights into high peak current in-cloud lightning events during thunderstorms. *Geophysical Research Letters*, *42*, 6836–6843. <https://doi.org/10.1002/2015GL065047>
- Marshall, R. A. (2012). An improved model of the lightning electromagnetic field interaction with the D-region ionosphere. *Journal of Geophysical Research*, *117*, A03316. <https://doi.org/10.1029/2011ja017408>
- Marshall, R. A., da Silva, C. L., & Pasko, V. P. (2015). Elve doublets and compact intracloud discharges. *Geophysical Research Letters*, *42*, 6112–6119. <https://doi.org/10.1002/2015GL064862>
- Marshall, T., Schulz, W., Karunarathna, N., Karunarathne, S., Stolzenburg, M., Vergeiner, C., & Warner, T. (2014). On the percentage of lightning flashes that begin with initial breakdown pulses. *Journal of Geophysical Research: Atmospheres*, *119*, 445–460. <https://doi.org/10.1002/2013JD020854>
- Mende, S. B., Frey, H. U., Hsu, R. R., Su, H. T., Chen, A. B., Lee, L. C., et al. (2005). D-region ionization by lightning-induced electromagnetic pulses. *Journal of Geophysical Research*, *110*, A11312. <https://doi.org/10.1029/2005JA011064>
- Miyasato, R., Fukunishi, H., Takahashi, Y., & Taylor, M. J. (2003). Energy estimation of electrons producing sprite halos using array photometer data. *Journal of Atmospheric and Solar-Terrestrial Physics*, *65*(5), 573–581. [https://doi.org/10.1016/S1364-6826\(02\)00322-X](https://doi.org/10.1016/S1364-6826(02)00322-X)
- Mussa, R., & Ciaccio, G. (2012). Observation of ELVES at the Pierre Auger Observatory. *The European Physical Journal Plus*, *127*(8), 94. <https://doi.org/10.1140/epjp/i2012-12094-x>
- Nesbitt, S. W., Salio, P. V., Varble, A., Trapp, R. J., Roberts, R. R., Dominguez, F., et al. (2017). Improving high impact weather and climate prediction for societal resilience in Subtropical South America: Proyecto RELAMPAGO-CACTI. *American Geophysical Union, Fall Meeting 2017, abstract #H41K-06*.
- Neubert, T., Crosby, N. B., Huang, T.-Y., & Rycroft, M. J. (2009). ASIM—An instrument suite for the International Space Station, *AIP Conference Proceedings* (vol. 1118, pp. 8–12): AIP. <https://doi.org/10.1063/1.3137718>
- Newsome, R. T., & Inan, U. S. (2010). Free-running ground-based photometric array imaging of transient luminous events. *Journal of Geophysical Research*, *115*, A00E41. <https://doi.org/10.1029/2009JA014834>
- Rakov, V. A., & Uman, M. A. (1998). Review and evaluation of lightning return stroke models including some aspects of their application. *IEEE Transactions on Electromagnetic Compatibility*, *40*(4), 403–426. <https://doi.org/10.1109/15.736202>
- Rasmussen, K. L., Zuluaga, M. D., & Houze, R. A. (2014). Severe convection and lightning in subtropical South America. *Geophysical Research Letters*, *41*(20), 7359–7366. <https://doi.org/10.1002/2014GL061767>
- Rosado, J., Blanco, F., & Arqueros, F. (2014). On the absolute value of the air-fluorescence yield. *Astroparticle Physics*, *55*, 51–62. <https://doi.org/10.1016/J.ASTROPARTPHYS.2014.02.003>
- Taranenko, Y. N., Inan, U. S., & Bell, T. F. (1993). Interaction with the lower ionosphere of electromagnetic pulses from lightning: Heating, attachment, and ionization. *Geophysical Research Letters*, *20*(15), 1539–1542. <https://doi.org/10.1029/93GL01696>



- Valk, F., Aints, M., Paris, P., Plank, T., Maksimov, J., & Tamm, A. (2010). Measurement of collisional quenching rate of nitrogen states  $N_2(C^3\Pi_u, \mu = 0)$  and  $N_2^+(B^2\Sigma_g^+, \mu = 0)$ . *Journal of Physics D: Applied Physics*, *43*, 385202. <https://doi.org/10.1088/0022-3727/43/38/385202>
- van der Velde, O. A., & Montanyà, J. (2016). Statistics and variability of the altitude of elves. *Geophysical Research Letters*, *43*, 5467–5474. <https://doi.org/10.1002/2016GL068719>
- Veronis, G., Pasko, V. P., & Inan, U. S. (1999). Characteristics of mesospheric optical emissions produced by lightning discharges. *Journal of Geophysical Research*, *104*(A6), 12,645–12,656. <http://doi.wiley.com/10.1029/1999JA900129>
- Virts, K. S., Wallace, J. M., Hutchins, M. L., Holzworth, R. H., Virts, K. S., Wallace, J. M., et al. (2013). Highlights of a new ground-based, hourly global lightning climatology. *Bulletin of the American Meteorological Society*, *94*(9), 1381–1391. <https://doi.org/10.1175/BAMS-D-12-00082.1>
- Zipser, E. J., Cecil, D. J., Liu, C., Nesbitt, S. W., & Yorty, D. P. (2006). Where are the most intense thunderstorms on Earth? *Bulletin of the American Meteorological Society*, *87*(8), 1057–1071. <https://doi.org/10.1175/BAMS-87-8-1057>